Theoretical Analysis of Molecular Diffusion in Pressure-Driven Laminar Flow in Microfluidic Channels

Andrew Evan Kamholz and Paul Yager
Department of Bioengineering, University of Washington, Seattle, Washington 98195 USA

ABSTRACT The T-sensor is a microfluidic analytical device that operates at low Reynolds numbers to ensure entirely laminar flow. Diffusion of molecules between streams flowing side by side may be observed directly. The pressure-driven velocity profile in the duct-shaped device influences diffusive transport in ways that affect the use of the T-sensor to measure molecular properties. The primary effect is a position-dependent variation in the extent of diffusion that occurs due to the distribution of residence time among different fluid laminae. A more detailed characterization reveals that resultant secondary concentration gradients yield variations in the scaling behavior between diffusive displacement and elapsed time in different regions of the channel. In this study, the time-dependent evolution of analyte distribution has been quantified using a combination of one- and two-dimensional models. The results include an accurate portrayal of the shape of the interdiffusion region in a representative T-sensor assay, calculation of the diffusive scaling law across the width of the channel, and quantification of artifacts that occur when making diffusion coefficient measurements in the T-sensor.

INTRODUCTION

Microfluidic devices and components have recently been adopted in useful analytical instruments. Examples include dynamic cell separators (Wang et al., 2000), surface patterning of cells and proteins (Chiu et al., 2000), high-throughput nucleic acid analysis (Shi et al., 1999), and mass spectrometer delivery modules (Chan et al., 1999, Li et al., 2000). In nearly every microfluidic format, diffusion of the analytes or particles of interest is a fundamental aspect of the device operation. Two prominent manifestations of diffusive transport in microfluidics are band-broadening in capillary electrophoresis (Liu et al., 1992) and surface gradient formation by diffusion-limited deposition (Folch and Toner, 1998).

One device in which diffusion plays a crucial role is the T-sensor (Brody et al., 1997; Kamholz et al., 1999; Weigl and Yager, 1999). Used initially as a diagnostic device for chemical assays, the T-sensor utilizes the interdiffusion of analyte and indicator from two or more input streams to produce a signal change that can be correlated with a physical parameter, most often analyte concentration (Fig. 1). Because of the very low Reynolds numbers of the system (typically less than 1), the flow is strictly laminar and transport between input streams occurs only via diffusion. Note that this description is also applicable to the H-filter, a similar microfluidic device designed for sample preconditioning sensors (Weigl and Yager, 1999).

Using a T-sensor differs from flow injection analysis (FIA) in that the former assumes continuous sample input, whereas the latter relies on bolus injection (Ruzicka and Hansen, 1988). FIA has been used to make many practical measurements, including the molecular weight of macromolecules (Murugaiah and Synovec, 1992), the concentration of small molecules (Greenway et al., 1999), and fluorimetric assay determinations (Hodder et al., 1997). The steady-state sample input of the T-sensor allows for a different experimental methodology in which an optical detector, such as a camera, monitors an indicator property across the channel at some distance downstream. Because the flow is constant, weak signals, as from a dilute fluorescent analyte, can be detected through signal integration. Unlike FIA, for which sample dispersion and diffusion have been well quantified (Ruzicka and Hansen, 1988), the phenomena specific to pressure-driven side-by-side flow in a microchannel with continuous input are only beginning to be quantified (Ismagilov et al., 2000; Kamholz et al., 1999).

Hydrodynamics of pressure-driven flow

Many microfluidic applications, most notably capillary electrophoresis, utilize electroosmotic flow to generate fluid motion, resulting in a blunt velocity profile (Tallarek et al., 2000). In many instances, however, it is preferable to use pressure-driven flow because of the relative ease and flexibility of implementation and insensitivity to surface contamination, ionic strength, and pH. Such flow in a microfluidic rectangular-shaped channel generates additional complexity in the distribution of analytes and indicators because of the parabolic velocity gradient across one or both cross-sectional dimensions. All molecules in the channel, whether injected as a bolus or continuously, experience a position-dependent distribution in residence time. The breadth of such a distribution is reduced by diffusion across the velocity gradient and, therefore, is highly dependent on molecular species.

In the simplest form of the T-sensor, two fluids are input side-by-side and a signal from an interdiffusion event be-

Received for publication 28 July 2000 and in final form 3 October 2000.
Address reprint requests to Dr. Paul Yager, University of Washington, Department of Bioengineering, Box 352255, Seattle, WA 98195. Tel.: 206-543-6126; Fax: 206-543-6124; E-mail: yagerp@u.washington.edu.

0006-3495/01/01/155/06 $2.00

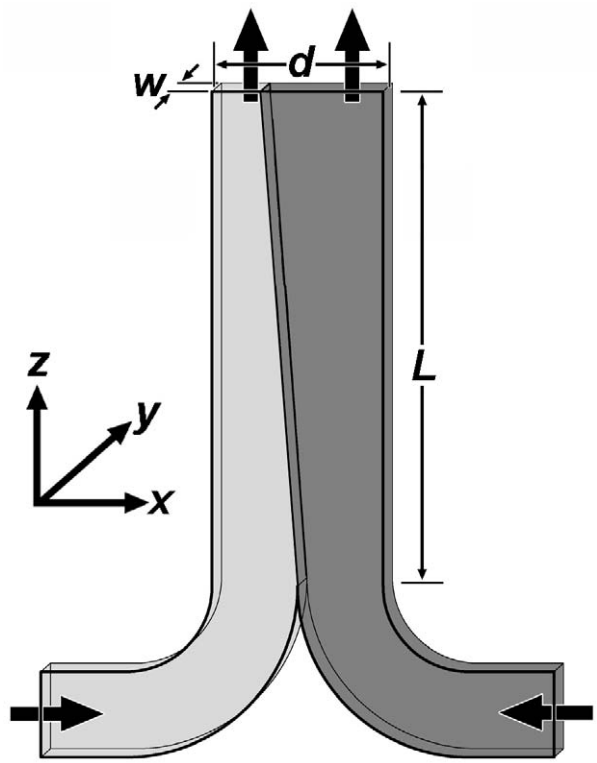

FIGURE 1 Conceptual rendering of the simplest form of the T-sensor. Two fluid inputs enter through channels at the bottom. In the case shown here, the fluid on the right contains a diffusible analyte (dark gray) that spreads across the *d*-dimension as flow proceeds along the channel length. During operation, measurements of optical signal are made a distance downstream, *L*, after significant interdiffusion has occurred.

tween sample constituent molecules is detected at some distance downstream (Fig. 1). For a rectangular channel with an aspect ratio greater than ~4, the velocity profile will be parabolic across the narrow dimension (called width, or *w*) and largely uniform across the majority of the wider dimension (called the diffusion dimension, or *d*) (Happel and Brenner, 1973). For channels with an aspect ratio, *d*/*w*, greater than 20, the velocity profile across *d* is unchanging for at least 90% of its length. T-sensors typically have aspect ratios greater than 6; this study considered one with an aspect ratio of 2.4 and others with aspect ratios well over 100.

One common application of the T-sensor is the measurement of diffusion coefficient. In practice, this is done most conveniently in the orientation shown in Fig. 1 using a fluorescently labeled analyte. Using traditional epifluorescence microscopy, the fluorescence intensity profile can be measured at a particular distance downstream. Then, a previously described one-dimensional model (Kamholz et al., 1999) can be used to fit empirical data to determine the apparent diffusion coefficient of the analyte. Typical experimental data with model fits for bovine serum albumin (BSA) are shown in Fig. 2.

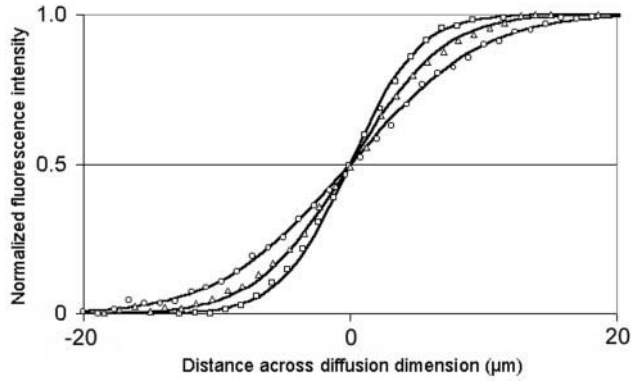

FIGURE 2 Experimental data with one-dimensional numerical fits for the diffusion of BSA in a T-sensor. The protocol and method of analysis have been described elsewhere (Kamholz et al., 1999). The device dimensions were $d = 2405\ \mu$m and $w = 10\ \mu$m, and the total input flow rates were 250 nl/s (○), 500 nl/s (△), and 1000 nl/s (□). Fits (——) used a diffusion coefficient of 6.5×10^{-7} cm^2/s. These data are representative of a concurrent experimental study that demonstrates the empirical determination of diffusion coefficient for a range of molecules of interest (manuscript in preparation).

The parabolic velocity profile will generate a substantial distribution in residence time across *w*. This results in a phenomenon previously identified as the butterfly effect (Kamholz et al., 1999), in which the extent of diffusion in the *d*-direction is a function of the location across *w* (and the resulting shape of the interdiffusion region resembles a butterfly or hourglass). The butterfly effect in a T-sensor was recently directly observed for the first time (Ismagilov et al., 2000); fluorescence generated from binding between calcium ions and an indicator was resolved in three dimensions using confocal microscopy.

Measurements in T-sensors are typically made using conventional epifluorescence microscopy, which does not offer the same spatial resolution (through *w*) as confocal microscopy. Rather, transmitted or emitted light is integrated along *w*, depending, in part, on the depth of focus of the objective lens. Therefore, any nonuniformity along *w* may manifest in the form of an artifact, as the apparent spatial distribution of analyte is an average of a complicated two-dimensional distribution.

Ismagilov et al. (2000) also demonstrated an important and nonintuitive characteristic of mass diffusivity in pressure-driven flow. Einstein's equation of Brownian motion (Einstein, 1956) states that

$$x = (2D\tau)^{1/2}, \tag{1}$$

where x is the root-mean-square distance traversed by a molecule during the time interval τ for a given diffusion coefficient D. The scaling behavior for distance versus time for a constant diffusivity therefore follows a one-half power law. In the classic Lévêque solution (Lévêque, 1928), it was demonstrated that thermal diffusivity normal to the surface

of a channel (and only very close to the surface as determined as a function of the Péclet number) obeys a one-third power law instead of one-half. Ismagilov et al. (2000), incorporating the natural analogy between thermal and mass diffusivity, extended the Lévêque solution to demonstrate that diffusion parallel to and near the surface in a flowing system should also be described by a one-third power law. Furthermore, they demonstrated this phenomenon experimentally in a T-sensor. It is of paramount importance to note that this difference in scaling law is not due to an actual change in the nature of diffusion but rather is a skewed diffusive distribution that is a consequence of the three-dimensional hydrodynamics of pressure-driven channel flow. All molecules in the system undergo conventional Brownian motion, but the net flux down concentration gradients perpendicular to flow is position dependent. As can be seen in Fig. 3, the scaling law difference results from secondary concentration gradients that develop across w as a consequence of fluid convection in the z-direction. This process is dependent on the relative time scales of convection and diffusion; the Péclet number can therefore be used as an indicator. Under nonflowing conditions, the secondary gradients would not form and the traditional one-half diffusive scaling law would apply across the entire w-dimension. In accordance with the conservation of mass, one would predict that the power law in some other part of the channel must exceed one-half to balance the decrease seen at the wall. As is demonstrated later in this study in a detailed numerical simulation, the power law does, in fact, exceed one-half in between the center of the channel (at $0.5w$) and the wall. The effects should be considered in all microfluidic devices in which diffusive transport affects function.

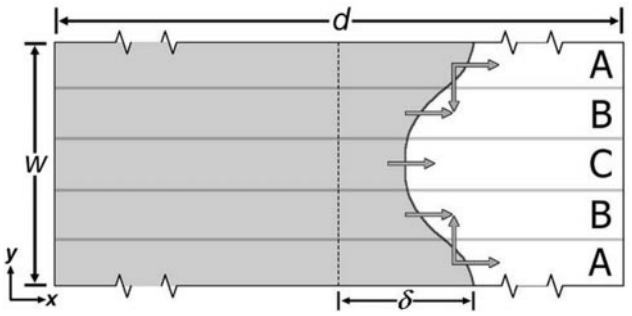

FIGURE 3 Depiction of the shape of the interdiffusion zone in a microfluidic channel when $d > w$ (aspect ratio of ~4 or greater). The flow direction is into the page. The diffusible analyte (gray) starts on the left side of the channel with the original fluid interface shown by the dotted vertical line. The butterfly effect, caused by the parabolic velocity profile across w, is shown in the shape of the interface at some arbitrary distance downstream. The function $\delta(y)$ is a measure of the distance between the original fluid interface and the current interface, as determined by an arbitrary concentration cutoff value. The gray arrows indicate regions of net analyte flux by diffusion, caused by either the primary concentration gradient between the left and ride side of the channel or by the secondary concentration gradients across the w-dimension caused by the butterfly effect. In all three regions (A, B, and C), there is net diffusion to the right caused by the primary concentration gradient. In region C, there is no net diffusion in the w-direction because there is no concentration gradient in this direction. In region A, there is a net flux of analyte (by diffusion) into the interior of the channel because there is a secondary concentration gradient. Region B is the recipient of this flux of material from region A. The result, demonstrated later in this study, is that the displacement of material by diffusion follows the traditional one-half power law in region C, but is less than one half in region A and greater than one half in region B.

METHODS

This study presents a numerical analysis of simulated analyte diffusion in pressure-driven flow. One portion of this work characterizes the diffusive scaling law across the width of a device, allowing accurate prediction of true spatial distributions of diffusing molecules. The other portion of this study simulates measurements made in a T-sensor and quantifies how the nonuniform diffusive scaling laws lead to artifacts in the measurement of molecular diffusion. Both parts of this study utilize a new two-dimensional model that describes pressure-driven flow in a microfluidic device.

Development of the two-dimensional model

The two-dimensional model is distinguished from a full three-dimensional model in that it has all of its nodes arranged within one channel cross section (in the d-w plane) rather than spaced along the length of the channel. Nevertheless, the model is able to describe flow in a T-sensor because of the steady-state nature of the input. In T-sensor flow, there are no significant concentration gradients along the axis of flow such as those in a bolus-injection scenario. Therefore, it is possible to use the length axis as the independent variable of integration.

Solutions using the two-dimensional model begin with the equation of continuity for an incompressible fluid (Bird et al., 1960):

$$\frac{\partial c_N}{\partial t} + \left(v_x \frac{\partial c_N}{\partial x} + v_y \frac{\partial c_N}{\partial y} + v_z \frac{\partial c_N}{\partial z}\right) = D_N\left(\frac{\partial^2 c_N}{\partial x^2} + \frac{\partial^2 c_N}{\partial y^2} + \frac{\partial^2 c_N}{\partial z^2}\right) + R_N, \quad (3)$$

where the coordinate axes are as in Fig. 1, c is the concentration of species N, v is velocity, D is diffusion coefficient of species N, and R is the production or elimination of species N by chemical reaction. Because flow in the T-sensor is steady state, the time-dependent term is zero. This ignores any potential entry effects, a phenomenon whose significance is currently being investigated (manuscript in preparation). Because the flow is strictly laminar at such low Reynolds numbers, all fluid velocities in the x- and y-directions are zero. Axial diffusion (in the z-direction) can also be neglected due to the steady-state input. The simulations conducted for this study did not include any chemical reaction, although modeling of a representative reaction has been demonstrated in the past (Kamholz et al., 1999). Application of these assumptions leads to

$$v_z \frac{\partial c_N}{\partial z} = D_N\left(\frac{\partial^2 c_N}{\partial x^2} + \frac{\partial^2 c_N}{\partial y^2}\right). \quad (4)$$

When discretized to a two-dimensional mesh, concentration as a function of position downstream (z-dimension) can be solved using common finite-differencing techniques (Finlayson, 1980). The velocity at each node is solved from the conservation of momentum (assuming uniform viscosity) and employing a no-slip condition at the walls. The wall boundary condition calls for no flux orthogonal to the surface but allows diffusion of analytes from the interior neighboring node. A more thorough boundary

condition would allow diffusion both with the interior and laterally (along the surface of the wall). However, this is more difficult to implement because it requires simultaneous solution of the concentrations at the entire wall surface. The exclusion of surface diffusion at the wall introduces a small error into the model that can be compensated by using a large number of nodes. The model was custom-coded on MATLAB and used its internal ordinary differential equation solver on a PC with a 450-MHz Celeron processor. Coarsely meshed solutions typically took a fraction of an hour whereas finely meshed solutions typically took several days.

Numerical analysis of the shape of the interdiffusion zone

The diffusive scaling law as a function of location across the w-dimension was determined by characterization of a finely meshed two-dimensional numerical simulation by the method of analysis demonstrated by Ismagilov et al. (2000). Briefly, Eq. 1 is used to find the power law behavior that relates the diffusive displacement to the elapsed time. The displacement is determined by calculating the function $\delta(y)$, the distance between the original fluid interface, and an arbitrary cutoff value for concentration (Fig. 3). The elapsed time is proportional to the distance downstream. The scaling law at each location across the w-dimension is determined by finding the slope of the line for δ plotted against distance downstream on a log-log scale.

The two-dimensional model was set up to simulate an experimental system similar to that analyzed by Ismagilov et al. (2000). The modeled diffusing analyte was calcium with a diffusion coefficient of 1.2×10^{-5} cm^2/s. The channel dimensions were $d = 260$ μm and $w = 110$ μm with a total length of 4 mm. The total flow rate was 2.2 μl/s, yielding an average interdiffusion time of $\sim$0.05 s.

Numerical simulation of measurements of diffusing analytes in the T-sensor

As discussed above, the nonuniformity across the w-dimension caused by the parabolic velocity profile may induce artifacts when making T-sensor measurements. Such artifacts were studied by using a combination of one- and two-dimensional simulations. The two-dimensional model was used to generate sets of simulated data for the diffusion of analytes in the T-sensor as in the configuration of Fig. 1. Such simulations consider the nonuniformity across the w-dimension induced by the parabolic velocity profile. Each set of two-dimensional data was then linearly summed over the w-dimension, mimicking the way that real data is collected in T-sensor experiments. Possible nonuniformity in the collection of light was neglected.

After summing the two-dimensional model sets, the one-dimensional model was used to find the best fit for apparent diffusion coefficient. Again, this mimics the way that experimental data is normally analyzed in the T-sensor. By completing this protocol over a range of parameters, it was possible to determine the severity of the system artifacts under various circumstances. This study was completed for two molecules: the small molecule fluorescein biotin ($D = 3.4 \times 10^{-6}$ cm^2/s) and the protein BSA ($D = 6.5 \times 10^{-7}$ cm^2/s). A substantial flow rate range was simulated, as were two different device widths: $w = 10$ μm and $w = 20$ μm. The diffusion dimension (d) was 2405 μm. The selections of molecules and device geometry were based on an accompanying experimental study (manuscript in preparation).

RESULTS AND DISCUSSION

The analysis of the simulations has led to a quantitative description of analyte diffusion in pressure-driven flow.

Quantification of diffusive scaling laws

The results of the two-dimensional numerical simulation of calcium diffusion in the T-sensor are shown in Fig. 4. Generated from model results, the top of Fig. 4 shows the manifestation of the butterfly effect; the shape of the diffusion front curves as flow proceeds downstream. Contour concentration plots at specific planes downstream (bottom of Fig. 4) show the effect more clearly.

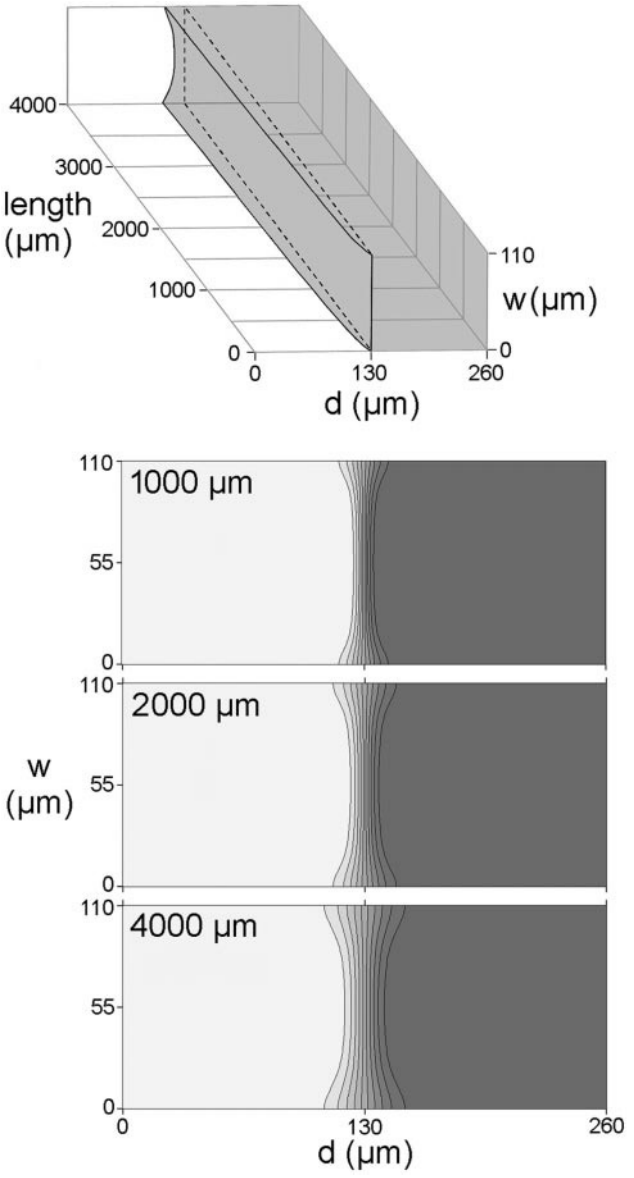

FIGURE 4 Numerical results from two-dimensional simulations of a T-sensor experiment. The analyte is calcium (gray) starting on the right side of the channel with $D = 1.2 \times 10^{-5}$ cm^2/s. The top image shows a composite rendering of the shape of the interdiffusion zone, with the front drawn at a concentration value of 10% of the bulk calcium concentration. The original fluid interface is shown with a dotted line. The bottom set of images shows individual interdiffusion contour plots at particular distances downstream.

The analysis of the diffusive scaling law across the *w*-dimension is shown in Fig. 5. Following the techniques developed by Ismagilov et al. (2000), the top of Fig. 5 shows representative plots of the diffusive displacement function δ versus distance downstream. The slopes of these lines are equivalent to the power law at each location across *w*. Summarized in the bottom of Fig. 5, the diffusive scaling shows a one-third power law at the wall of the channel and a one-half power law at the channel center (0.5 fractional distance at 0.5*w*). These results are in agreement with those obtained by Ismagilov et al. (2000) by both theoretical and empirical means. In addition, this study also quantifies the power law in the interval between these extremes. As anticipated by the qualitative argument presented in Fig. 3, the diffusive scaling does exceed a one-half power law between the channel center and wall, reaching a maximum value of 0.53 at one-sixth of the distance from the wall to the channel middle.

Simulated diffusion coefficient measurements

The results of the numerical simulations of diffusion coefficient measurement of fluorescein biotin and BSA in the T-sensor are shown in Fig. 6. The manifestation of artifacts is dependent on both the diffusion coefficients of the molecules and the distance across the velocity gradient (i.e., the width). As predicted, a smaller diffusion coefficient and a large width produce a more dramatic impact of the butterfly effect as the analyte undergoes less equilibrating diffusion across *w*. It is reasonable to assume that increasingly wide devices would lead to more striking consequences from the butterfly effect. It is again stressed that this does not reflect a change in the nature of diffusion itself, but only a change in the analyte distribution that leads to a shift in the apparent behavior.

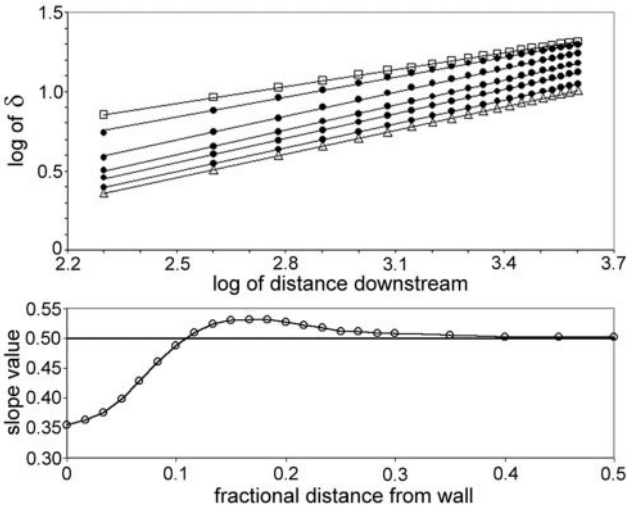

FIGURE 5 (*Top*) Plot of the width of the interdiffusion zone (δ) versus distance downstream. □, measurements made at the wall (fractional distance = 0); △, measurements made in the middle of the channel (at w = 55 μm, fractional distance = 0.5). The remainder of the data sets were taken at fractional distances of 0.05, 0.1, 0.15, 0.2, and 0.3. Many other data sets were taken but omitted from the figure for clarity. The lines show the best fit over the entire range of data shown. (*Bottom*) Best linear-fit values for the slope over the middle 10 points of each line from the top image. The slope value does not quite reach one-third at the wall because of limitations in the boundary conditions of the two-dimensional model (see Methods). The results demonstrate the one-half power law at the channel center (fractional distance of 0.5) and one-third power at the wall.

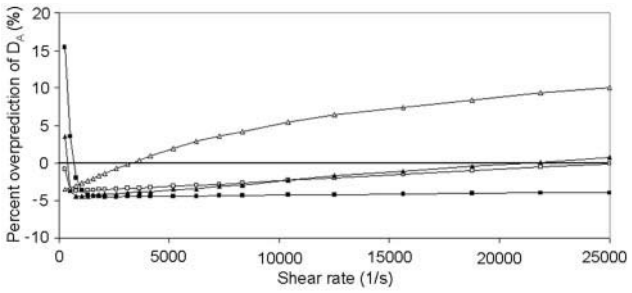

FIGURE 6 Results of analysis of two-dimensional model data using the one-dimensional model. The data were generated by selecting a diffusion coefficient (3.4×10^{-6} cm^2/s for fluorescein-biotin and 6.5×10^{-7} cm^2/s for BSA) and conducting simulations at various flow rates. Each data set was summed across w, mimicking data collection in an actual T-sensor experiment, and was then fit to the best diffusion coefficient with the one-dimensional model. Squares are in a channel with w = 10 μm; triangles are w = 20 μm. Open symbols are for BSA; solid symbols are for biotin. The flow rate range for the 10-μm device is 10–1000 nl/s, and the range for the 20-μm device is 40–4000 nl/s. Calculation of shear rate utilizes the assumption that the flow is between infinite parallel plates (Andrade, 1985).

Another interesting feature of Fig. 6 is that, at very slow flow rates (and shear rates), the model apparently greatly overpredicts diffusivity. This is presumably due of the contribution of analyte diffusing into the interior from the very slowly moving laminae near the walls (refer to Fig. 3). When the flow is slow enough, there is sufficient time for the interior portions of the channel to receive a significant amount of analyte from the wall regions. At the approach to zero flow rate, the phenomenon becomes a singularity because there is an infinite amount of time for such exchange; the apparent diffusivity in such cases approaches infinity. The flux of material to the interior depends on the (actual) diffusion coefficient of the analyte, and thus the BSA requires even slower flow rates for the singularity to appear. At fast flow rates, the time for such exchange with the interior is vastly reduced and this phenomenon becomes insignificant. This phenomenon, as predicted by the numerical simulations, has not yet been verified experimentally and therefore may possibly be due to limitations of the models.

CONCLUSIONS

This work presents a quantitative study of the spatial distribution of diffusing analytes in a microfluidic pressure-

driven device using numerical simulations. The verification of the extension of the Lévêque solution (Lévêque, 1928) to diffusion parallel to the surface as proposed by Ismagilov et al. (2000) has implications for all microfluidic devices. In macro-scale devices, the reduction of apparent diffusivity also exists but encompasses a vanishingly small fraction of the channel. In microfluidics, however, the effect can encompass the entire channel. It is of importance particularly in devices in which diffusion to and along surfaces is significant, such as surface patterning methods, many DNA chips, and applications utilizing self-assembling monolayers.

The T-sensor can be used to empirically measure the concentrations of analytes by constructing calibration curves. However, quantitative measurements of molecular parameters and design of optimal devices require an accurate theoretical analysis of mass transport in the microfluidic device. This work extends the previous T-sensor study (Kamholz et al., 1999) by quantifying the influence of the velocity profile on the distribution of analytes. Most importantly, the two-dimensional analysis has established the magnitude of artifacts that arise in the measurement of diffusion coefficients in the T-sensor.

We thank Prof. Bruce Finlayson (Department of Chemical Engineering, University of Washington) for considerable assistance with developing the two-dimensional model. Most importantly, we acknowledge the continual support of the members of the Yager research group, particularly Mr. Eric Schilling, Dr. Katerina Macounova, Ms. Catherine Cabrera, Mr. Anson Hatch, Mr. Kenneth Hawkins, and Mr. Matthew Munson for essential scientific discussions.

This work was supported by DARPA contract N660001–97-C-8632.

REFERENCES

Andrade, J. 1985. Principles of Protein Adsorption. Plenum Press, New York.

Bird, R., W. Stewart, and E. Lightfoot. 1960. Transport Phenomena. John Wiley and Sons, New York.

Brody, J. P., A. E. Kamholz, and P. Yager. 1997. Prominent microscopic effects in microfabricated fluidic analysis systems. *Proc. Micro. Nanofabricated Electro-Opt. Mech. Systems Biomed. Environ. Appl.* 103–110.

Chan, J. H., A. T. Timperman, D. Qin, and R. Aebersold. 1999. Microfabricated polymer devices for automated sample delivery of peptides for analysis by electrospray ionization tandem mass spectrometry. *Anal. Chem.* 71:4437–4444.

Chiu, D. T., N. L. Jeon, S. Huang, R. S. Kane, C. J. Wargo, I. S. Choi, D. E. Ingber, and G. M. Whitesides. 2000. Patterned deposition of cells and proteins onto surfaces by using three-dimensional microfluidic systems. *Proc. Natl. Acad. Sci. U.S.A.* 97:2408–2413.

Einstein, A. 1956. Investigations on the Theory of the Brownian Movement. Dover Publications.

Finlayson, B. A. 1980. Nonlinear Analysis in Chemical Engineering. McGraw-Hill, New York.

Folch, A., and M. Toner. 1998. Cellular micropatterns on biocompatible materials. *Biotechnol. Prog.* 14:388–392.

Greenway, G. M., S. J. Haswell, and P. H. Petsul. 1999. Characterisation of a micro-total analytical system for the determination of nitrite with spectrophotometric detection. *Anal. Chim. Acta.* 387:1–10.

Happel, J., and H. Brenner. 1973. Low Reynolds Number Hydrodynamics. Noordhoff.

Hodder, P. S., G. Blankenstein, and J. Ruzicka. 1997. Microfabricated flow chamber for fluorescence-based chemistries and stopped-flow injection cytometry. *Analyst.* 122:883–887.

Ismagilov, R. F., A. D. Stroock, P. J. A. Kenis, and G. Whitesides. 2000. Experimental and theoretical scaling laws for transverse diffusive broadening in two-phase laminar flows in microchannels. *Appl. Phys. Lett.* 76:2376–2378.

Kamholz, A. E., B. H. Weigl, B. A. Finlayson, and P. Yager. 1999. Quantitative analysis of molecular interaction in a microfluidic channel: the T-sensor. *Anal. Chem.* 71:5340–5347.

Lévêque, M. A. 1928. Les lois de la transmission de chaleur par convection. *Ann. Mines.* 13:201–299, 305–362, 381–415.

Li, J., J. F. Kelly, I. Chernushevich, D. J. Harrison, and P. Thibault. 2000. Separation and identification of peptides from gel-isolated membrane proteins using a microfabricated device for combined capillary electrophoresis/nanoelectrospray mass spectrometry. *Anal. Chem.* 72: 599–609.

Liu, J., V. Dolnik, Y. Z. Hsieh, and M. Novotny. 1992. Experimental evaluation of the separation efficiency in capillary. *Anal. Chem.* 64: 1328–1336.

Murugaiah, V., and R. E. Synovec. 1992. Radial measurement of hydrodynamically generated concentration profiles for molecular-weight determination. *Anal. Chem.* 64:2130–2137.

Ruzicka, J., and E. H. Hansen. 1988. Flow Injection Analysis. J. Wiley, New York.

Shi, Y., P. C. Simpson, J. R. Scherer, D. Wexler, C. Skibola, M. T. Smith, and R. A. Mathies. 1999. Radial capillary array electrophoresis microplate and scanner for high-performance nucleic acid analysis. *Anal. Chem.* 71:5354–5361.

Tallarek, U., E. Rapp, T. Scheenen, E. Bayer, and H. Van As. 2000. Electroosmotic and pressure-driven flow in open and packed capillaries. *Anal. Chem.* 72:2292–2301.

Wang, X. B., J. Yang, Y. Huang, J. Vykoukal, F. F. Becker, and P. R. Gascoyne. 2000. Cell separation by dielectrophoretic field-flow-fractionation. *Anal. Chem.* 72:832–839.

Weigl, B., and P. Yager. 1999. Microfluidic diffusion-based separation and detection. *Science.* 283:346–347.